V-band Bull's eye antenna for multiple discretely steerable beams

V-band Bull's Eye Antenna for Multiple Discretely-Steerable Beams

Clement J. Vourch [1], Timothy D. Drysdale [2]

[1] Electronics & Nanoscale Engineering Division, University of Glasgow, Glasgow, G12 8LT, UK
[2] Department of Engineering and Innovation, The Open University, Milton Keynes, MK7 6AA, UK
*tim.drysdale@open.ac.uk

Abstract: We present a new approach to designing V-band Bull's eye antenna so as to produce multiple beams, which are either fixed or discretely steerable. Bull's eye antennas comprise concentric rings around a subwavelength aperture. Beam deflection is accomplished by adjusting the effective spacing of the rings, which we explain in terms of the coupling angle to free space and surface waves. We show that multiple beams can be obtained from a single antenna, with the deflection of each beam being controlled independently by the relevant portion of the ring pattern. We demonstrate the principle through rigorous full-wave simulations of two-beam antennas with symmetrical and asymmetrical shifts, and give experimental results for a prototype milled in aluminium, with two separate fixed beams each deflected 16° to either side of the broadside. We also propose means to obtain up to six different beam arrangements during operation by mechanically rotating a plate containing a special six-sector ring pattern. Our simulated example gives three patterns, a single broadside beam or two beams each deflected by 8° or 15°. The radiation efficiency of the antenna is 97%, and the gain of a single undeflected beam is 18.1dBi.

1. Introduction

Bull's eye antennas were first used at optical wavelengths to enhance the transmission from subwavelength apertures associated with single mode optical fibres, light-emitting diodes and semiconductor lasers [1]. The principle applies equally well to out-coupling from single-mode waveguides in the micro- and millimetre-wave bands. A millimetre-wave antenna based on this principle is of interest because it offers a very low profile and good directivity [2-4], yielding similar performance to a horn antenna for a fraction of the size. Compact, directive antennas are important where space and energy use are at a premium, for example, communicating between members of a swarm of small satellites or point-to-point communications within existing infrastructures. For convenience, the main beam should be able to be designed so that communication links can be established even when the sides of the small satellite or building walls are known not to be facing each other; split into multiple beams where simultaneous communication is desired with more than two parties, and/or steered to accommodate changes in the relative positions of the transmitter and the receiver. The possibility of changing the direction of the main beam by shifting the centre of the rings has been reported at optical frequencies [5] and at millimetre-wave frequencies [6-8]. This concept is called the holographic principle and allows beam steering and beam forming by scattering the surface currents with specific surface impedance patterns

[9,10]. In the case of the Bull's eye antenna, those patterns are periodic, metallic gratings. In our earlier work [6], we showed that shifting the rings deflects the main beam in both the E-plane and H-plane, but the amount of deflection was fixed for a given design and not adjustable after the antenna was manufactured.

In this Paper, we extend our analysis of the shifting effect to show that it is consistent with the coupling angle between free space waves and surface wave using a periodic grating. We exploit localised nature of the leaky waves to extend the design to give multiple beams and discretely steerable single or multiple beams. Specifically, we experimentally demonstrate dual beam operation and propose and simulate a mechanical tuning scheme for live or "on-the-fly" beam steering of one (or two beams) to six (or three) discrete angles. For consistency in presentation, we begin with the same antenna design that we used in [6].

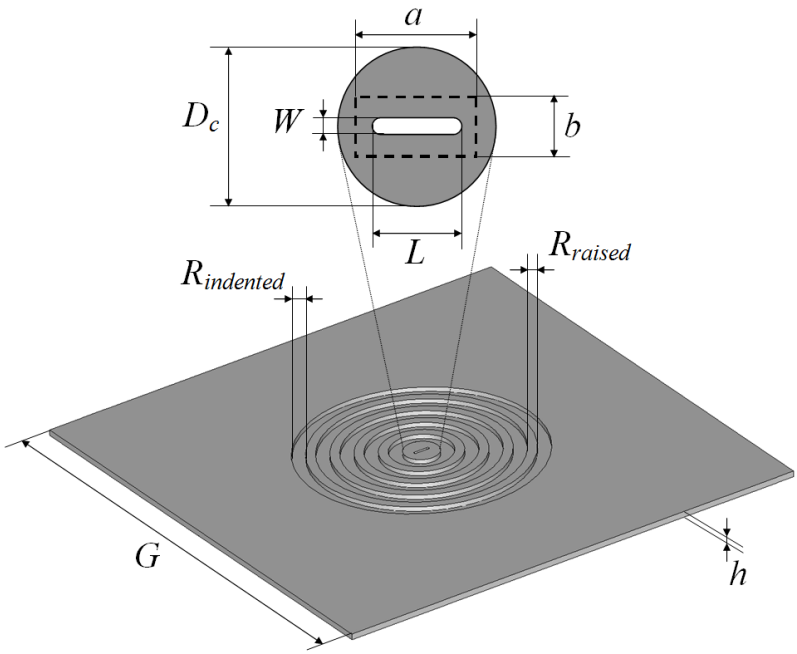

Fig. 1. *Design dimensions of the V-band Bull's eye antenna. The dotted line shows the position of the WR-15 waveguide feed.*

The design dimensions of an antenna with a single beam emitted along the broadside are defined in Figure 1, and listed in Table 1. Note that the antenna performance is insensitive to *G*, as long as the ground plane is large enough to contain the indented rings.

Table 1 Dimensions of the studied Bull's eye structure in millimetres

G	*a*	*b*	$R_{indented}$	R_{raised}	*W*	*L*	D_c	*h*
100	3.76	1.88	2.67	1.86	0.530	3.40	7.12	3.20

We assume the antenna is fed from the rear by a WR-15 rectangular waveguide, with the long side of the waveguide parallel to *L*. This gives operating frequencies that are centred around 60GHz. The rectangular aperture results in a linear polarisation. A WR-15 feed is not the only possible option for this antenna, but since it is convenient for our experimental setup we do not explore other feed options in this Paper.

A linearly polarised antenna is adequate for communications in the 60GHz band because there is minimal Faraday rotation of the polarisation [11,12]. In any case, atmospheric losses are high in the 60GHz band, so we expect most uses of our antenna to be in short ground-ground, or space-space communications links where Faraday rotation does not occur. Further, linear polarisation is desirable from the point of view of enabling polarisation-based multiplexing for additional channel capacity.

Other antennas in the 60GHz range achieve wide impedance bandwidth (33%) with modest gain (7.5dBi) [13] or use arrays of dielectric resonators fed by substrate integrated waveguides [14] for increased gain (16.5dBi). The use of dielectrics in such antennas reduces the radiation efficiency due to substrate losses in the complex waveguide networks, needed to feed enough antennas to form an array with high directivity. On the other hand, we anticipate that widespread adoption of 60 GHz communications systems will drive demand for alternative solutions that are efficient, with high gain, yet inexpensive and straightforward to manufacture.

The Paper is organised as follows. In Section 2 we explain the operation of the antenna in terms of leaky waves, using as the example the E-plane shift of a single beam. In Section 3, we show how to achieve multiple beams, and show that each of the beams in a two-beam design is individually deflectable. In Section 4 we present measurement results for a symmetrical double-shifted ring structure. We present the design of a mechanically steerable Bull's eye antenna using a sectorial rotating plate in Section 5, and our conclusions in Section 6.

2. Single Structure Ring Shift

In this Section we simulate the deflection of the main beam when the rings are shifted in a single direction. We begin by showing the effect, and then explain it in the later part of the section. The scheme for shifting the rings is as follows. The centre of each raised ring is shifted such that the n^{th} ring from the centre is shifted by $n \times Shift$, where *Shift* is the offset of the innermost raised ring. *Shift* is a free parameter in the limit that the rings can be produced in a conventional milling machine. This limits *Shift* to a maximum value of $R_{indended}$, which is 2.67mm for our design in Table 1. Our shifting scheme retains the

same dimension for the raised part of the ridge, but allows the indented portion to change size. This approach is preferable to the opposite approach (indented size stays the same size, raised ring changes size), which reduces the degree of shift, reduces the gain, and introduces unwanted side lobes in the radiation pattern (results not shown here).

We carried out a parametric study in the E- and H-plane for *Shift* ranging from 0mm to 2.67mm, in seven steps (0, 0.50, 1.0, 1.5, 2.0, 2.5, 2.67mm) to establish that the shifts are monotonic, but we present results only for shift of 0, 1.0, 2.0 and 2.67mm for clarity in the figures in later sections. All our simulations are conducted with CST Microwave Studio's time domain solver. The waveguide at the rear of the antenna is excited with a single-mode waveport and the metal is modelled as Aluminium with conductivity of 3.538×10^{7} $S.m^{-1}$. We use magnetic (or electric) walls for single or asymmetrical double shifts in the E-plane (or H-plane) to halve the simulation domain, and for symmetrical double shifts we use magnetic and electric walls to quarter the simulation domain. The far-field polar radiation patterns are plotted in Figure 2 for *Shift* = 0 and 2.67mm in the form of linear gain as a function of angle, with a perspective view of half of the associated Bull's eye structure. The purpose of Figure 2 is to make clear the link between an offset in the rings and the deflection in the beam. Further details of the E- and H-plane shift can be found in [6].

The performance at some example intermediate deflections is summarised in Table 2. The deflection angle is approximately proportional to the *Shift* value, but the gain reduces from 18.1dBi to 13.5dBi due to a slight increase in power radiated away from the main beam, rather than a change in the 3dB beam-width. Any secondary lobes remain below - 10dBi, except when *Shift* = 2mm (structure C), where an extra lobe at -25° rises at -6.8dB due to resonances in the surface currents (not shown here).

Table 2 Angle deflection and gain according to single E-plane ring shift

Ring shift (mm)	0.0	0.50	1.0	1.5	2.0	2.5	2.67
Deflection angle (°)	*0.0*	*5.1*	*9.9*	*12.7*	*15.4*	*18.4*	*20.0*
Gain (dBi)	*18.1*	*18.4*	*17.9*	*16.5*	*16.6*	*13.4*	*13.5*

We attribute the beam deflection of shifted rings to the action of leaky waves [15]. In order to show that this explanation is consistent with our results, we compare the deflection angle of the main beam, to the coupling angle given by a standard momentum-matching equation. Momentum matching equations are typically used to predict coupling angles for one-dimensional gratings in the optical regime and metal gratings in the microwave and millimetre-wave bands [16].

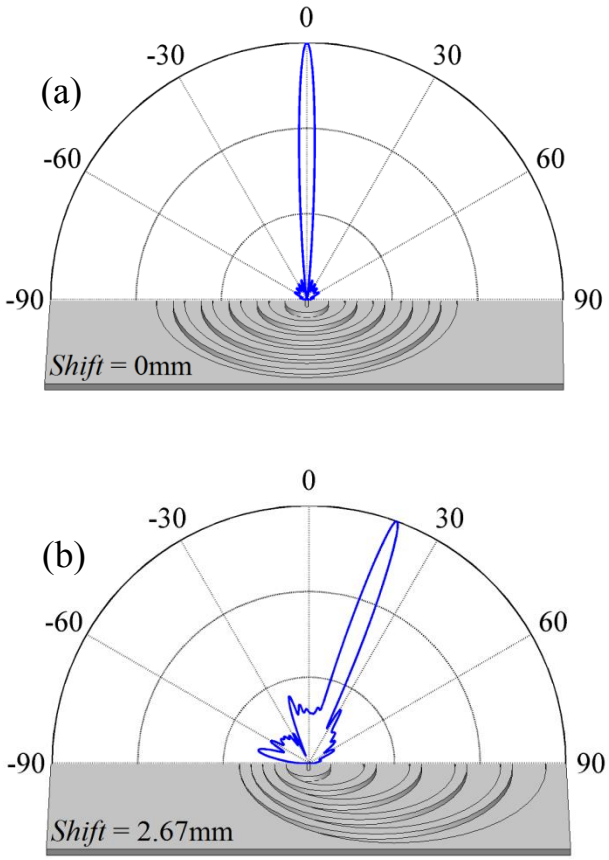

Fig. 2. *Qualitative illustration of how the Bull's eye antenna's main beam is deflected by shifting the rings. Each subfigure shows a polar plot of linear gain above a 3D view of half of the antenna*
a Standard design with unshifted rings yielding a single main beam directed along the broadside (maximum gain of 18.1dBi)
b Design with shifted rings that deflects the single main beam by 20.0° (for a maximum gain of 13.5dBi). In both cases the radiation efficiency is 97% and the aperture efficiency is 6%.

By considering the cross section of our antenna along the main axis parallel to the direction of the shift, we can define a one-dimensional grating that is approximately equivalent to our antenna. Naturally we do not expect this to represent accurately the behaviour of the antenna under all conditions. For example, we expect the one-dimensional grating model to be less valid at larger shift values due to the loss of rotational symmetry, and the change in the effective filling factor. Nonetheless, a straightforward model helps elucidate the mechanism that dominates the antenna's performance. For a grating, the relationship between the surface wave phase constant β, the radiation angle θ, and the period of the grating Λ is given by, for the n = -1 space harmonic:

$$\beta = k_0 \sin\theta + \frac{2\pi}{\Lambda} \tag{1}$$

where $k_0 = 2\pi/\lambda_0$ is the free-space wavenumber. In this frequency range and since the grating is a good conductive metal, the surface wave phase constant is expected to be close to the free space wavenumber $\beta \approx k_0$, and non radiative (slow wave) with $\beta > k_0$.

Now we are interested in two questions: first, how good is a one-dimensional grating model at predicting the performance of a Bull's eye antenna, and second, what effect does the grating profile and filling factor have on the coupling angle? We address these two questions by plotting in Figure 3 the deflection angle from an modified (optimised) and a canonical (un-optimised) Bull's eye antenna (modelled with CST Microwave Studio in 3D), their equivalent one-dimensional gratings (modelled with Rigorous Coupled Wave Analysis [17]), and the deflection angle predicted for a sinusoidal grating of the same period. The sinusoidal grating is the black line, the (un-optimised) canonical grating and antenna are the black markers, and the (optimised) modified grating and antenna are the white markers. Immediately it is clear that all five sets of results follow qualitatively the same trend. To emphasise the uniting role that leaky waves play in governing all the results that we present in Figure 3, we plot, as a colormap, surface wave phase constant β as a function of the effective grating period Λ, defined as the initial period Λ_0 plus the parameter *Shift* ($\Lambda = \Lambda_0 + Shift$), and the incident angle, by using equation (1). Aside from some deviation due to the rectangular grating profile and variable fill factor – which is known to affect the coupling angle [18] - and the extra dimension in the antenna rings versus a simple one-dimensional grating.

To address the second question, we now discuss in more detail each of the sets of results in Figure 3. As expected, the surface wave (non radiative) has a phase velocity slightly lower than free space ($\beta > k_0$ and $\beta \approx k_0$). The one-dimensional canonical grating (simulated by RCWA) is remarkably close to the free space wavenumber. The (un-optimised) canonical Bull's eye antenna (Λ_0 = 5mm, filling factor = 0.50 to 0.33, black circles, shows a similar trend while showing discrepancies with the grating ranging from 0.7 to 2.98°, with an increasing trend (clearly visible from Λ = 5.25 to 6.5mm) indicating the loss of rotational symmetry.

We plot as white markers, the deflection angle of the modified (optimised) grating (Λ_0 = 4.53mm, filling factor = 0.41 to 0.26, white square markers) and the deflection angle of the modified (optimised) Bull's eye antenna (Λ_0 = 4.53mm, filling factor = 0.41 to 0.26, white circle markers).

The modified grating's filling factor ranges from 0.41 to 0.26, creating narrower ridges with higher spatial harmonics than the canonical structure. We note that it is understood that β can vary slightly when the grating profile contains a significant amount of higher spatial harmonics [19], and we expect this to begin to strain the analogy to the one-dimensional gratings at smaller shift values. The variation in β can

be noticed as a general trend that the reduction of the filling factor tends to increase the surface wave phase constant and subsequently the deflection angle.

Nonetheless, this simplified model is a useful way to understand the operation of the antenna, and gives an efficient approach to predicting the performance of a Bull's eye antenna, prior to conducting numerical simulations of optimised structures.

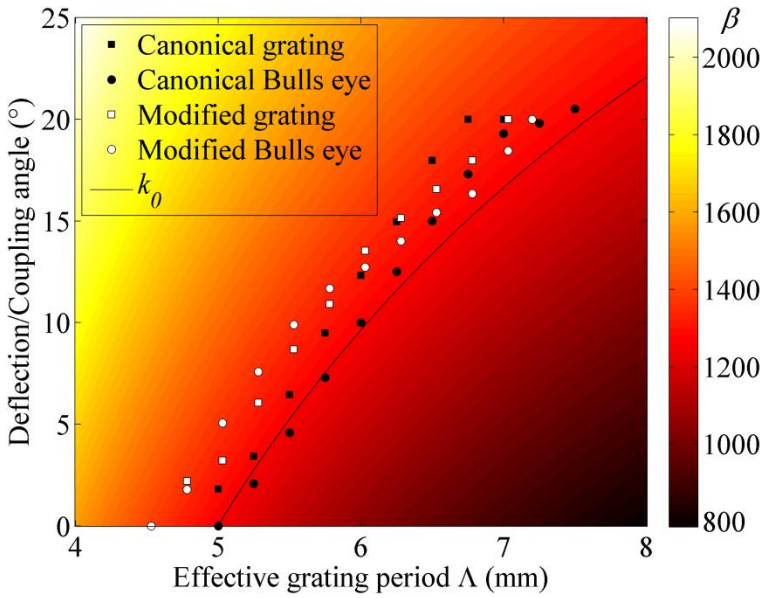

Fig. 3. *Plot comparing the simulated deflection angle of optimised ("modified") and un-optimised ("canonical") Bull's eye antennas to the coupling angle of the associated one dimensional rectangular profile gratings, as a function of the effective grating period $\Lambda = \Lambda_0 + Shift$. The solid black line is the free-space wavenumber, and the colourmap shows how the coupling angle and the grating period relate to the surface wave phase constant.*

As expected, the surface wave (non radiative) has a phase velocity slightly lower than free space ($\beta > k_0$), following an average isoline of $\beta = 1330$.

The H-plane shift has also been investigated, and is reported in [6]. We only note here that the E- and H-plane shift performance is similar, allowing beam shifting even in polarisation diversity schemes where both E- and H-plane shifts are needed.

3. Double Structure Ring Shift

We now explore the possibility of generating multiple main beams at one time. To do this, we put a different pattern on different sides of the antenna. This allows greater flexibility in future communications systems where more than one link is required simultaneously, yet with each individual link benefiting from a directive beam for power efficiency. The rest of this Section is organised as follows. In Section 3.1

we first investigate symmetrical patterns so as to steer both beams equally, and then in Section 3.2 we investigate asymmetrical patterns so as to deflect each beam by a different amount.

3.1. Symmetrical shift

Two symmetrical structures have been investigated. The first has its ring centres shifted within the E-plane for positive shift values. Figure 4 shows the radiation patterns for *Shift* = 0, 1.0, 2.0 and 2.67mm. Figure 4.(1) shows the creation of two primary separate lobes, with deflection angle ranging from 0° to 18.6°.

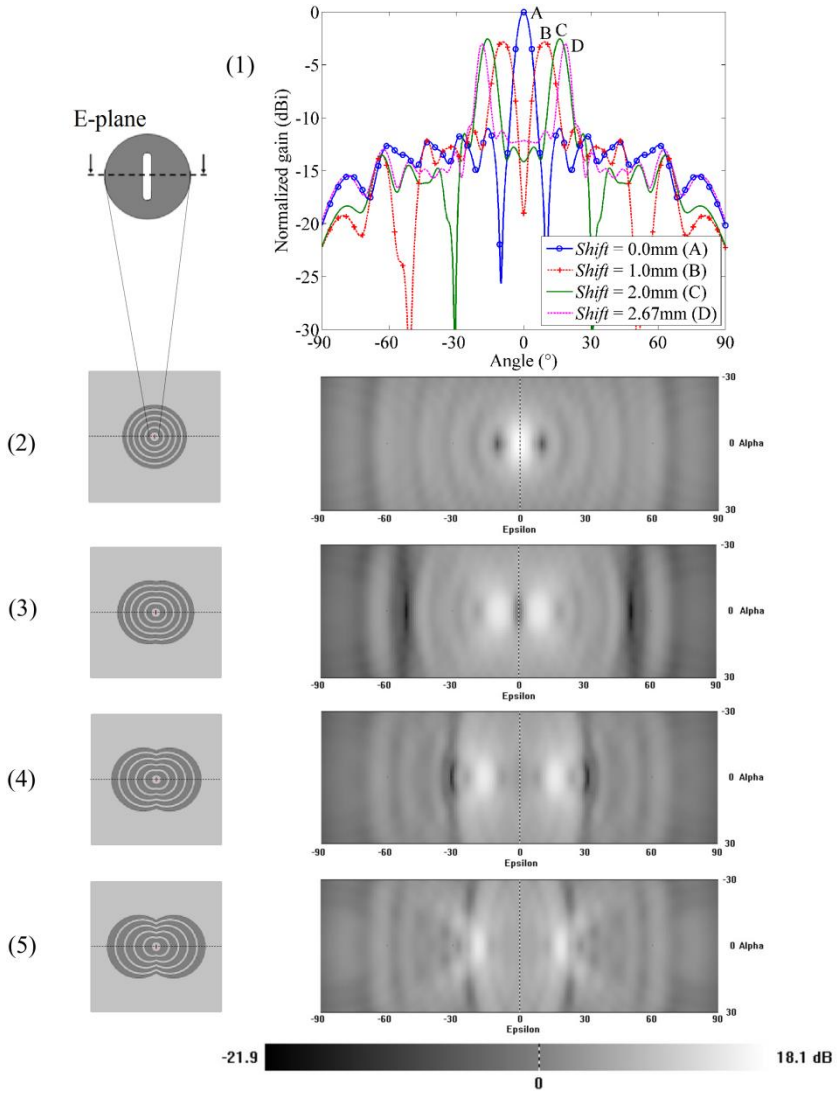

Fig. 4. *E-plane radiation patterns (1); and E-plane double positive shift rings structure with corresponding 2D radiation pattern for 0.0 (2), 1.0 (3), 2.0 (4) and 2.67mm (5) shift.*

The gain drops from 18.1dBi to about 15.1dBi, which is expected because of equal splitting of the power between the two main radiation beams (full efficiency is maintained overall). The secondary lobes

stay below -8dBi. Table 3 shows the deflection angle, the maximum gain and the -3dB beamwidth within the E-plane as a function of *Shift*.

Table 3 Deflection angle, gain and beamwidth according to double E-plane positive ring shift

Ring shift (mm)	0.0	1.0	2.0	2.67
Deflection angle (°)	*0.0*	*9.3*	*16.1*	*18.6*
Gain (dBi)	*18.1*	*15.3*	*15.6*	*15.1*
-3dB beamwidth (°)	*6.7*	*8.9*	*7.3*	*5.1*

We then investigated the H-plane positive double shift structure for *Shift* = 0, 1.0, 2.0 and 2.67mm. Figure 5 shows the radiation pattern for the structure.

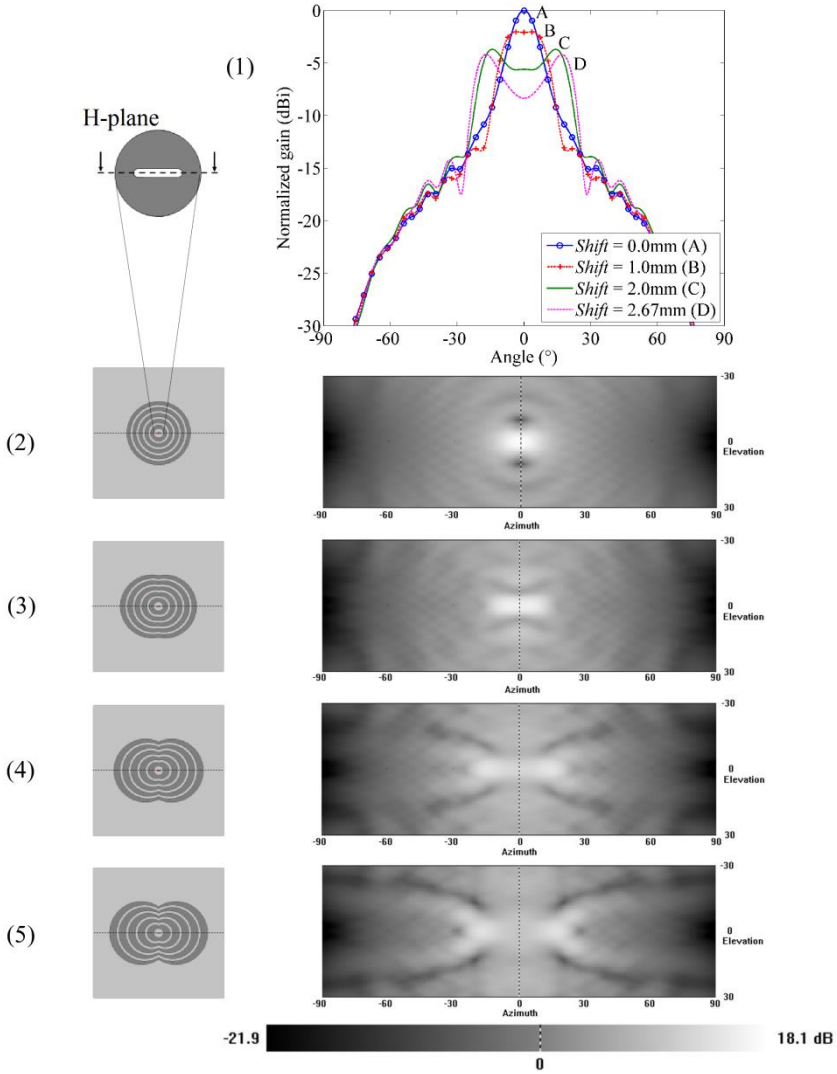

Fig. 5. *H-plane radiation patterns (1); and H-plane double positive shift rings structure with corresponding 2D radiation pattern for 0.0 (2), 1.0 (3), 2.0 (4) and 2.67mm (5) shift.*

Two main lobes are still created, but the separation is not as obvious as for the E-plane until *Shift* ≥ 2mm. Table 4 shows the deflection angle, the maximum gain and the -3dB beamwidth within the H-plane according to the shift of the rings. If double lobes are required, the E-plane is preferable.

Table 4 Deflection angle, gain and beamwidth according to double H-plane positive ring shift

Ring shift (mm)	0.0	1.0	2.0	2.67
Deflection angle (°)	*0.0*	*3.3*	*14.3*	*17.0*
Gain (dBi)	*18.1*	*16.0*	*14.4*	*13.9*
Beamwidth (°)	*13.2*	*22.1*	*40.3*	*15.2*

3.2. Asymmetrical shift

Since we established in the previous sections that the positive-shifted half of the E-plane pattern predominantly determines the beam properties, we expect that two different positive patterns can be combined to create beams that are deflected by different amounts. In other words, for E-plane positive shifts, each half of the pattern interacts with a different region of the surface current so we expect the beam deflection to be independently adjustable. This is desirable because it simplifies the design of an antenna to meet an arbitrary specification. We illustrate the independence of the two beams by example. We keep one beam along the normal direction (*Shift* = 0mm) and progressively increase the deflection of the other beam by offsets of *Shift* = 0, 1.0, 2.0 and 2.67mm. Figure 6 shows the radiation patterns and plan view schematics of the ring patterns. The E-plane radiation patterns in Figure 6.(1) show the deflection of the shifted lobe ranges from 0° to 21°.

Adding shift reduces the maximum gain to 10.1dBi, for the maximally shifted lobe at *Shift* = 2.67mm. On the other hand, the lobe that we did not want to deflect, remains within -0.5° and 1.6° of the broadside. The gain of the line of sight lobe also drops from 18.1dBi to 11.6dBi, as shown in Figure 6.(1). We attribute this to a small interaction of the currents on each side of the aperture. We did not optimise this design further, but we suggest introducing small un-patterned guard bands, or trenches, between the two gratings.

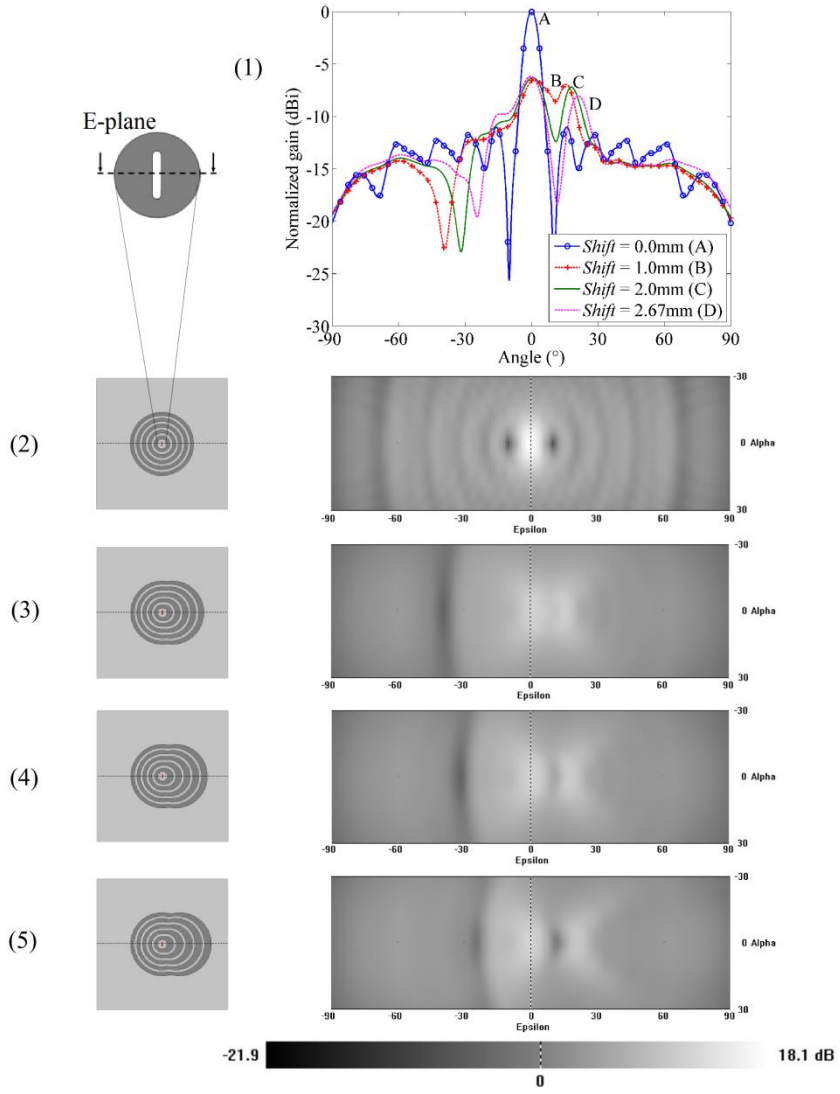

Fig. 6. *E-plane radiation patterns (1); and E-plane asymmetrical shift rings structure with corresponding 2D-projection radiation pattern for 0.0 (2), 1.0 (3), 2.0 (4) and 2.67mm (5) shift.*

4. Measurements

In order to experimentally demonstrate that multiple beams can be created, as we have proposed here, we manufactured an E-plane double positive shift Bull's eye antenna with *Shift* = 2.0mm, for an expected deflection of 16.1° on each side of the broadside. A 3-axis XYZ SM2000 CNC milling machine was used to create ring pattern on the aluminium plate. We measured the antenna radiation pattern inside a 4.5m × 4.5m × 4.0m anechoic antenna test chamber so as to avoid electromagnetic interference and parasitic reflections. The structure was mounted on a rotating stage taking measurements from -90° to +90°, in steps of 2°. Experimental S21 parameter data was acquired via an Agilent PNA (E8361A) with 500Hz IF bandwidth and averaging of 10 points per sample, with a linearly polarized 23dBi horn antenna (Custom Microwave, Inc., model HO15R), separated by 110cm (220λ) from the Bull's eye antenna under

test. Figure 7.(a) shows a photograph of the fabricated 2mm E-plane shift Bull's eye antenna and Figure 7.(b) shows the simulated and measured E-plane radiation patterns, after normalisation.

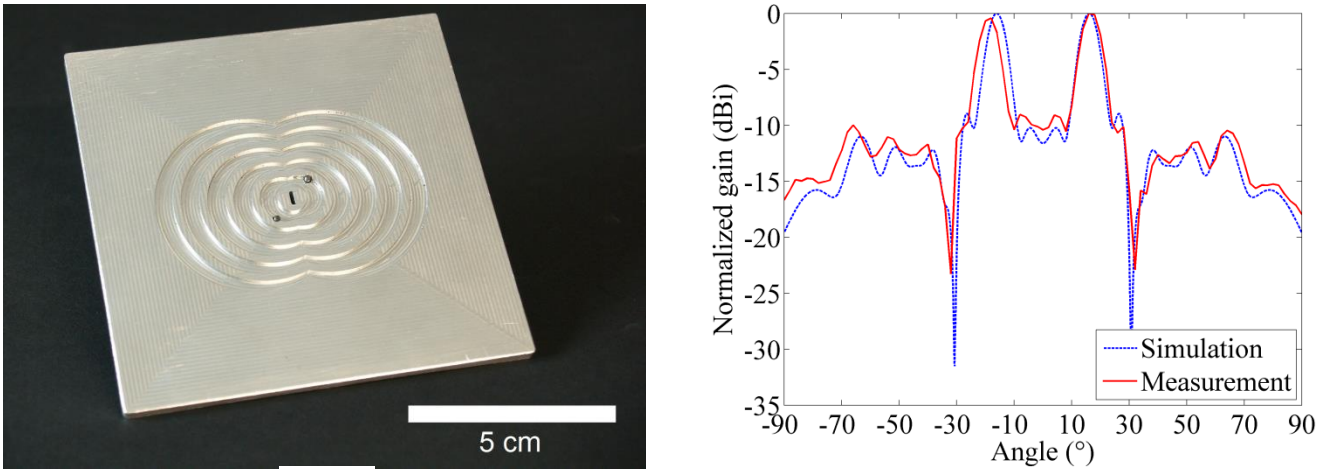

(a) (b)

Fig. 7. *a Fabricated 2mm E-plane shift Bull's eye antenna.*
b Normalized simulated and measured E-plane radiation pattern.

Figure 7.(b) shows good agreement between the two normalized E-plane radiation patterns. The measured main lobe on the negative angle side is offset by -2° from the simulation, while there is good agreement in the location of the secondary lobes at ±39°, ±52°, ±64°and ±80°, and nulls at ±30°. We attribute the small shift in the main lobe to fabrication tolerances in the production of the antenna.

5. Mechanical steering with sectorial structure

A beam steering capability is essential for point-to-point communications where there are multiple transceivers (such as consumer products in a domestic environment, or a constellation of small satellites or CubeSats in space). Electronic beam steering via phased arrays such as [20,21] is often fast, and ideal for short range communication where the environment varies rapidly but the link budget is not strained. However, electronic beam steering introduces losses through networks of splitters and phase shifters or delay lines [22]. A typical electronic phase shifter can introduce up to 3dB of insertion loss, reducing range by 30% for a given link budget. To counter this, mechanical steering systems have been proposed, such as mechanically tilting dielectric lenses [23], although these introduce a coupling loss between the feed horn and the lenses which is not present in a Bull's eye design.

For applications such as mobile backhaul, point-to-point communication in fixed (or reconfigurable) constellations of small satellites, and millimetre-wave radar, the overall link budget is often constrained. It is necessary to prioritise range and signal to noise ratio over speed of beam steering. For example, the

OLFAR CubeSat mission [24] can use the 59-71 GHz intersatellite service band for high bandwidth data-sharing between swarm members. Power budgets are strictly limited by the small size of the platform and therefore the higher transmission efficiency of a mechanical steering system is attractive because it allows the CubeSat constellation to cover a wider area yet still share high-bandwidth data.

For the Bull's eye antenna, a number of mechanical steering schemes are apparent – but most suffer from severe disadvantages in practice. For example, attempting to create individually-machined moving rings results in a complex mechanism that offsets any cost or space saving associated with the fixed version of the design. Instead we propose to sacrifice continuous tunability for a mechanically straightforward scheme with few moving parts.

Figure 8 shows the exploded view of our concept, which comprises three parts: an aluminium mask, a rotating plate with six sectors (60° each) each containing different ring patterns, and a fixed aluminium base including the subwavelength aperture. The aluminium mask is necessary to counterbalance the effect of an asymmetrical pattern along the unsteered-plane for each of the positions, i.e. for an antenna that steers in the E-plane, the sections of the antenna that would influence the H-plane should be masked, and vice-versa. The system for rotating the sectorial plate is note shown here, for simplicity. We suggest adding teeth to the outer teeth of the sectorial plate and using a geared drive to rotate it. Ball races can be built into the interface between the base and the sectorial plate, which will prevent friction without disrupting any surface current flows because they will away from the active surfaces.

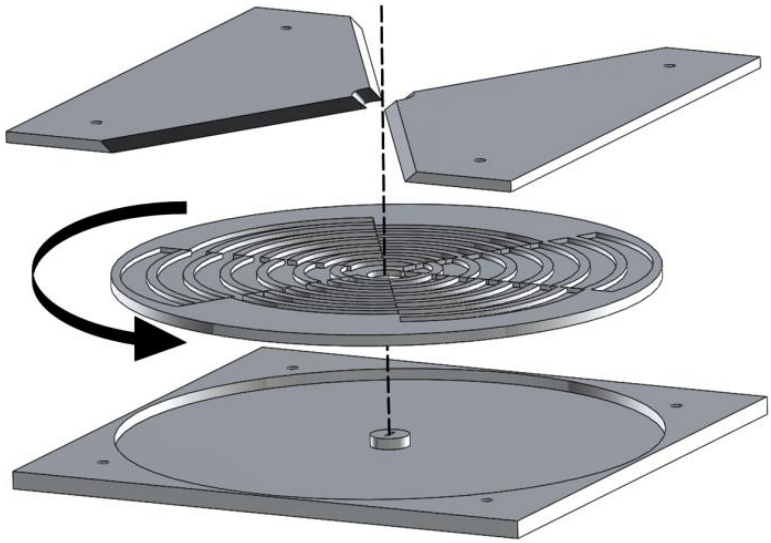

Fig. 8. *Exploded view of the 6-sector mechanical shift antenna with rotating plate.*

Figure 9 shows the simulated E-plane radiation pattern for the three positions (a), with corresponding structures (b). Figure 9.(b) also illustrates asymmetry of the structure on each side of the

E-plane. The three positions (*Shift* = 0mm, 1mm and 2mm) provide main beam deflection of 0°, ±7.9° and ±15.0° within the E-plane and a maximum gain of 16.2dBi, 14.9dBi and 15.1dBi.

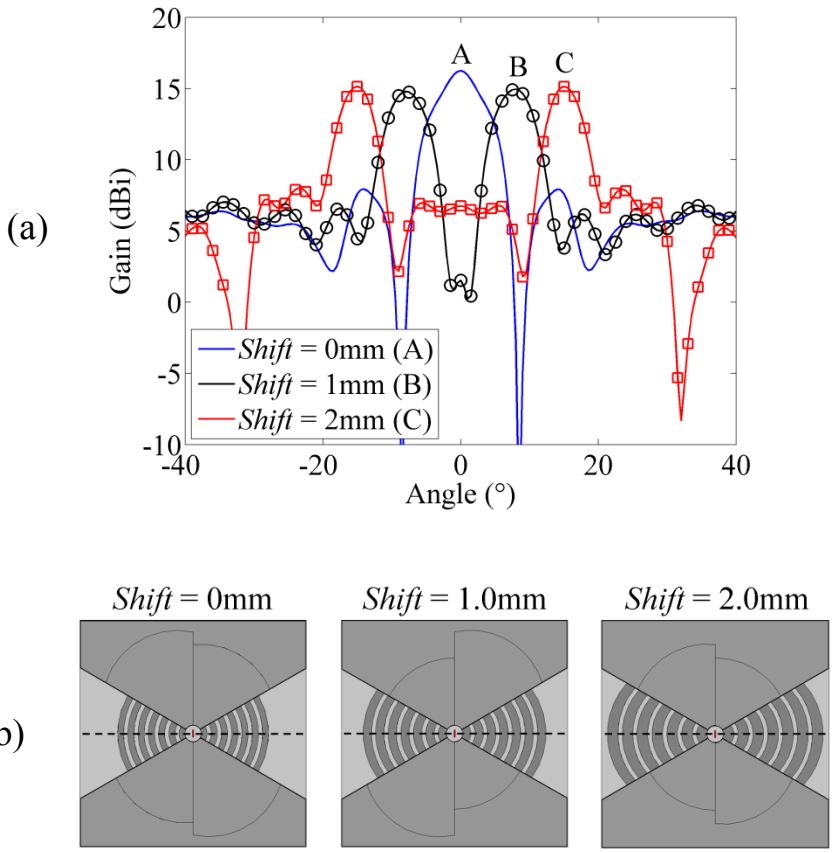

Fig. 9. *a E-plane radiation pattern for the three positions (0mm, 1mm and 2mm shift).*
b Corresponding structures (mask showed in transparency), where the dotted line represents the E-plane.

In results not shown here, we also designed a sectorial plate that allowed a single beam to be steered to -14.5°, -7.7°, 0°, +7.7° and +14.5°, with a maximum gain of 17.1dBi at ±7.7°.

6. Conclusion

We presented the design of Bull's eye antennas with deflected double beams in the E- and H-planes, and a mechanical scheme for making single and double beams discretely steerable during operation. We deflected the beam(s) by shifting the rings that surround the aperture. For a shift of 2.67mm in the E-plane, a single beam is deflected by 20°, yet retained a high-gain narrow beam (18.1dBi for an undeflected beam, 13.5dBi for a fully deflected beam) and a high radiation efficiency (97%). We explained the operation of the antenna in terms of leaky wave, showing that a simple one-dimensional grating model is sufficient to predict the deflection angle with minimal computational effort and reasonable accuracy. Since leaky wave coupling are a localised effect, it is possible to independently design different gratings on different sides of

the aperture, with each grating setting the deflection angle of its own beam. We experimentally validated this concept for an antenna that created two beams deflected to 16.1^{o} either side of the broadside, with a gain of 15.6dBi. Fixed designs could be useful in a number of static scenarios, but a steerable antenna would give more flexibility. While a number of mechanical steering schemes are possible for this type of antenna, many are likely to be mechanically impractical. We proposed a straightforward scheme based on a rotating plate with different patterns in six sectors, and a mask to prevent unwanted modifications to the beam-shape by the inactive portions of the sectorial plate. In the example design we presented, we can select between a single beam along the broadside, or two beams at either 7.9^{o} or 15.0^{o}. In another version, that we did not show, we could deflect a single beam to -14.5^{o}, -7.7^{o}, 0^{o}, $+7.7^{o}$, or $+14.5^{o}$, i.e. five different directions. The choice of angles is arbitrary. In summary, the Bull's eye antenna is compact, inexpensive, and flexible and we expect it to be useful in point to (multi-)point links in terrestrial and space-based applications.

7. Acknowledgments

We thank the staff of the University of Glasgow's mechanical workshop for making the Bull's eye antenna. TDD acknowledges support from EU FP7 IRSES project AdvIOT. CJV acknowledges support from a University of Glasgow James Watt Research Scholarship.

8. References

[1] Lezec, H.J., Degiron, A., Devaux, E., *et al*.: 'Beaming Light from a Subwavelength Aperture', Science 2, August 2002, **297**, (5582), pp. 820-822

[2] Beruete, M., Campillo, I., Dolado, J.S., *et al*.: 'Very low-profile "Bull's Eye" feeder antenna', IEEE Antennas and Wireless Propagation Letters, 2005, **4**, pp. 365-368

[3] Beruete, M., Beaskoetxea, U., Zehar, M., *et al*.: 'Terahertz Corrugated and Bull's-Eye Antennas', IEEE Trans. on Terahertz Science and Technology, November 2013, **3**, (6), pp. 740-747

[4] Beaskoetxea, U., Pacheco-Pena, V., Orazbayev, B., *et al*.: '77-GHz High-Gain Bull's-Eye Antenna With Sinusoidal Profile', IEEE Antennas and Wireless Propagation Letters, 2015, **14**, pp. 205-208

[5] Tetienne, J., Blanchard, R., Yu, N., *et al*.: 'Dipolar modeling and experimental demonstration of multi-beam plasmonic collimators', New J. Phys., May 2011, **13**, (5)

[6] Vourch, C.J., Drysdale, T.D.: 'V-Band "Bull's Eye" Antenna for CubeSat Applications', IEEE Antennas and Wireless Propagation Letters, 2014, **13**, pp. 1092-1095

[7] Minatti, G., Sabbadini, M., Maci, S.: 'Surface to leaky wave transformation in polarized metasurfaces', Proc. of 2013 URSI Int. Symp. on Electromagnetic Theory (EMTS), 20-24 May 2013, pp. 298-301

[8] Minatti, G., Faenzi, M., Martini, E., *et al*.: 'Modulated Metasurface Antennas for Space: Synthesis, Analysis and Realizations', IEEE Trans. on Antennas and Propagation, April 2015, **63**, (4), pp. 1288-1300

[9] ElSherbiny, M., Fathy, A.E., Rosen, A., *et al*.: 'Holographic Antenna Concept, Analysis and Parameters', IEEE Trans. on Antennas and Propagation, 2004, **52**, (3), pp. 830-839

[10] Rusch, C.: 'Holographic Antennas', in Cheng, Z.N. (Ed.): 'Handbook of Antenna Technologies' (Springer, 2015), pp. 1-31

[11] International Telecommunication Union, Recommendation ITU-R P.531-12, 'Ionospheric propagation data and prediction methods required for the design of satellite services and systems', September 2013

[12] Jehle, M., Ruegg, M., Zuberbuhler, L., *et al*.: 'Measurement of Ionospheric Faraday Rotation in Simulated and Real Spaceborne SAR Data', IEEE Trans. on Geoscience and Remote Sensing, May 2009, **47**, (5), pp. 1512-1523

[13] Ng, K.B., Wong, H., So, K.K., *et al*.: '60 GHz Plated Through Hole Printed Magneto-Electric Dipole Antenna', IEEE Trans. on Antennas and Propagation, July 2012, **60**, (7), pp. 3129-3136

[14] Li, Y., Luk, K.:'A 60-GHz Dense Dielectric Patch Antenna Array', IEEE Trans. on Antennas and Propagation, Feb. 2014, **62**, (2), pp. 960-963

[15] Jackson, D.R., Caloz, C., Itoh, T.: 'Leaky-Wave Antennas', Proc. of the IEEE, July 2012, **100**, (7), pp. 2194-2206,

[16] Hibbins, A.P., Sambles, J.R., Lawrence, C.R.: 'Grating-coupled surface plasmons at microwave frequencies', J. of Appl. Phys., 1999, **86**, (4), pp. 1791-1795

[17] Moharam, M.G., Gaylord, T.K.: 'Rigorous coupled-wave analysis of metallic surface-relief gratings', J. Opt. Soc. Am. A, 1986, **3**, (11), pp. 1780-1787

[18] Giannattasio, A., Hooper, I. R., Barnes, W. L.: 'Dependence on surface profile in grating-assisted coupling of light to surface plasmon-polaritons', Opt. Commun., May 2006, **261**, (2), pp. 291–295.

[19] Raether, H.: 'Surface plasmons on smooth and rough surfaces and on gratings' (Springer Tracts in Modern Physics, Vol. 111, Springer Berlin 1988)

[20] Emami, S., Wiser, R.F., Ali, E., *et al*.: 'A 60GHz CMOS phased-array transceiver pair for multi-Gb/s wireless communications', IEEE International Solid-State Circuits Conference Digest of Technical Papers (ISSCC), 20-24 Feb. 2011, pp. 164-166

[21] Natarajan, A., Reynolds, S.K., Ming-Da T., *et al*.: 'A Fully-Integrated 16-Element Phased-Array Receiver in SiGe BiCMOS for 60-GHz Communications', IEEE Journal of in Solid-State Circuits, May 2011, **46**, (5), pp. 1059-1075

[22] Ta, C.M., Skafidas, E., Evans, R.J., and Hoang, C.D.: 'A 60-GHz variable delay line on CMOS for steerable antennae in wireless communication systems', Canadian Conference on Electrical and Computer Engineering, 4-7 May 2008, pp. 1915-1918

[23] Costa, J.R., Lima, E.B., Fernandes, C.A.: 'Compact Beam-Steerable Lens Antenna for 60-GHz Wireless Communications', IEEE Transactions on Antennas and Propagation, October 2009, 57, (10), pp. 2926-2933

[24] Rajan, R.T., Engelen, S., Bentum, M., *et al*.: 'Orbiting Low Frequency Array for radio astronomy', IEEE Aerospace Conference, 5-12 March 2011, pp.1-11